

# Design of an imaging bolometer system for the large helical device

G. A. Wurden

*Los Alamos National Laboratory, Los Alamos, New Mexico, 87545*

B. J. Peterson and Shigeru Sudo

*National Institute for Fusion Science, Nagoya 464-01, Japan*

(Presented 15 May 1996)

We describe a radical design for a bolometer system employing infrared (IR) imaging of a segmented-matrix absorber in a cooled-pinhole camera geometry, which we will prototype and demonstrate on the large helical device (LHD).<sup>1</sup> LHD will be operational in early 1998, with an  $l=2$  superconducting winding, a major radius of 3.9 m, a minor radius of 0.5–0.65 m, and input powers ranging from 3 MW (steady state) to 30 MW (pulsed). The bolometer design parameters are determined by modeling the temperature of the foils making up the detection matrix using a two-dimensional time-dependent solution of the heat conduction equation. This design will give a steady-state bolometry capability, with modest (60 Hz) time resolution, while simultaneously providing hundreds of channels of spatial information. No wiring harnesses will be required, as the temperature-rise data is measured via a 12-bit,  $\pm 0.025$  °C resolution, 3–5  $\mu\text{m}$  band,  $256 \times 256$  pixel IR camera. The spatial data will be used to tomographically invert the profile of the highly shaped stellarator main plasma and divertor radiation, in conjunction with more conventional fanned arrays of traditional bolometers.

## I. INTRODUCTION

Bolometers are a standard magnetic fusion plasma diagnostic.<sup>2–5</sup> However, it is usually problematic to have a sufficient number of channels and views to accurately reconstruct the plasma radiation profile.<sup>6</sup> In addition, every discrete detector channel usually has 2–4 wire leads carrying low-level signals out through the vacuum interface, and this results in complicated wiring harnesses inside today's large, high-temperature, high nuclear-radiation environment devices, leading to high costs and complexity. It has been recently proposed to build a rad-hard imaging bolometer, using a segmented-absorber matrix,<sup>7</sup> combined with a pinhole-camera geometry and sensitive infrared (IR) camera, for the international thermonuclear experimental reactor (ITER) or tokamak physics experiment (TPX). The concept would allow several thousand channels of data, while at the same time using no wiring or wiring feedthrus across the vacuum interface. In this article we show refinements of this idea, as specifically implemented for the large helical device (LHD) geometry, access constraints, and power levels.

## II. GENERAL CONCEPT AND DESIGN CONSTRAINTS

We desire to build an imaging bolometer to provide radial and/or tangential views of the LHD plasma, which will operate with expected total plasma radiation levels from 1–30 MW, and over time scales from 10 s to almost steady-state plasma durations. LHD will be capable of diverted plasma operation, and, due to the geometry of the close-fitting helical coils, the only possible views of the main plasma always include sightlines through the “divertor region.”<sup>8</sup> This is a serious limitation when inverting the chordal information to obtain the (assumed) lower signal levels from the plasma core. The average plasma power density, assuming 100% radiation in the case of a 3 MW, 27 m<sup>3</sup> volume plasma, is only 0.11 W/cm<sup>3</sup>. Clearly, it is essential to

have sufficient sensitivity to easily see this expected signal level. At the same time, available port space on the vacuum vessel dictates distances and dimensions of an acceptably sized bolometer “canister” that will be mounted in-vacuum on a reentrant tube in order to approach the plasma as close as possible and thus maximize the incident radiation and resulting signal levels.

The heart of the design lies in constructing a heat absorber with fast time resolution, good sensitivity, long-term cooling, and the ability to image a radiation source. We consider a segmented matrix consisting of a thin metal foil sandwiched between two metal blocks drilled with matching arrays of holes exposing portions of the foil to both sides. One side (the front side) of the matrix views the plasma through a pinhole. The change in temperature of the exposed foils due to the radiation incident through the pinhole is detected by an IR camera which views the matrix from the side opposite the pinhole (back side) through an IR vacuum window. The foil is made as thin as possible with a material with low thermal conductivity for high sensitivity. The mask is made of a material of high thermal conductivity which, when water cooled, acts as a heat sink for the exposed foils. This prevents lateral heat flow from spilling onto adjacent pixels, while also allowing for cooling to prevent melting during long pulse operation. The pinhole shell will also be cooled to eliminate stray IR radiation from the housing.

As originally conceived,<sup>7</sup> the segmented absorber matrix would have been viewed from its front surface, and cooled from the back surface, which would allow a simpler design, with a more uniform cooling substrate. However, it was recognized that stray IR light from the inner wall of the hot armor in a plasma device would probably contaminate the desired optical IR-band signal. Consequently, we develop a more complicated “back-viewed and side-cooled” geometry matrix for LHD. We are willing to sacrifice some time resolution for superior spatial coverage in steady-state operation.

TABLE I. Material parameters at 20 °C. Temperature rise (uncooled, cooled, and rise time to 50% of final value) for 1.5 mm diameter, 2- $\mu$ m-thick foil segment, assuming a 3 MW plasma radiation source, with a 9.9-mm-diam pinhole in a 55° FOV pinhole camera located at 2 m distance from the plasma axis.

Foil material	$\rho$ density (gm/cm <sup>3</sup> )	$k$ conductivity (W/[cm °C])	$\kappa$ diffusivity (cm <sup>2</sup> /s)	$\frac{Q \cdot \delta t}{[Cp \cdot \rho \cdot V]}$ $\delta t=17$ ms (milli °C)	$\Delta T$ final cooled (milli °C)	$\tau$ rise time (ms)
Bismuth	9.78	0.079	0.065	275	306	15
SS 304	7.817	0.144	0.0387	92	195	20
Titanium	4.5	0.219	0.08	121	128	10
Nickel	8.91	0.909	0.229	84	31	3.5
Aluminum	2.7	2.37	0.975	138	12	0.8
Gold	19.3	3.16	1.27	134	9	0.55
Copper	8.9	3.99	1.166	98	7	0.6

We are restricted by the technology of today’s IR cameras to a temperature resolution of at best  $\pm 0.01$  °C with a frame rate of 1 kHz ( $\pm 0.025$  °C and 60 Hz with our Amber Engineering “Radiance-1” camera) with commercially available, state-of-the-art 12-bit digital video systems. This particular camera has been tested in magnetic fields of 0.01–0.06 T (Alcator and DIII-D vertical fields, a few meters outside the toroidal field coils) with no performance impairment. It operates in the 3–5  $\mu$ m infrared band. Expected foil temperature increases will be small, and the nominal operating temperature will be elevated slightly above room temperature.

### III. MODELING AND RESULTING DESIGN PARAMETERS

The choice of foil material depends on the expected heat load, the desired temperature rise, the foil’s opacity to the expected radiation, and the required time response. To model the transient temperature rise time, a time-dependent solution to the heat conduction equation (without radiation losses) for the cylindrical geometry of the foil segment has been used. We assume (and confirm) that the foil is sufficiently thin compared to its transverse (radial) cooling dimensions, so that we can neglect any time dependence of axial gradients between the front and back surface. For this case, we can use the model of an infinitely long rod, of radius  $b$ , which has a volumetric heat source turned on at time  $t=0$ , while the boundary of the rod is held clamped at a fixed temperature  $T=0$  °C. The incident power density is then assumed to be uniform throughout the foil. Additionally, we apply a uni-

form initial condition of  $T=0$  °C for the foil, and then obtain the thermal response as a function of time,<sup>9</sup> and radius from the center of the foil segment, at the surface of the foil given by Eq. (1)

$$T(r, t) = \frac{2}{b} \times \frac{Sf}{k \times \text{th}} \sum_{m=1}^{\infty} \left[ \frac{J_0(\beta_m \times r)}{J_1(\beta_m \times b)} \times \frac{1 - \exp[-\kappa(\beta_m)^2 \times t]}{(\beta_m)^3} \right], \quad (1)$$

where  $k$  is the thermal conductivity,  $\kappa$  is the thermal diffusivity,  $Sf$  is the incident power flux (W/cm<sup>2</sup>), and  $\beta_m$ ’s are the  $m^{\text{th}}$   $J_0$  Bessel function roots normalized by  $b$ , arising from the cylindrical geometry. Using this model we adjust the foil radius,  $b$ , and the foil thickness,  $\text{th}$ , for various metals to arrive at an optimum set of design parameters. Using thermal parameters of different metals (characterized by Ref. 10), the rise time and temperature for various foils are given in Table I. Materials with fast rise times (good heat transfer properties) result in a small temperature increase, relative to the uncooled case (for one video field time  $\delta t=17$  ms). This has resulted in our selection of bismuth for the foil material due to its low conductivity and heat capacity, resulting in higher thermal sensitivity to the incident power. The resulting foil segment parameters have  $b=0.75$  mm and  $\text{th}=2$   $\mu$ m. For a bismuth foil this gives a temperature rise of 0.36 °C with a rise time of 15 ms, matching the time resolution of the IR camera and exceeding its temperature sensitivity by a factor of  $\sim 15$ . The spatial resolution in the plasma is 13 cm,

TABLE II. For given temperature rise time ( $\tau=15$  ms), thickness (2  $\mu$ m), and material, the table shows the necessary diameter of the edge-cooled foil. Materials with faster heat conductivity require a larger distance to the “edge-cooled” boundary, to maintain the same temperature rise-time constraint. At the same time, larger diameter foils can be matched to a larger diameter pinhole, which puts a higher power density on each foil segment.

Foil material	$\Delta T$ final cooled (milli °C)	Pinhole diameter (mm)	Foil diameter (mm)	No. of macro pixels
Bi	306	9.9	1.5	16×16
SS 304	146	10.1	1.3	16×16
Ti	184	9.6	1.8	16×16
Ni	124	8.5	3.0	16×16
Al	484	13.1	6.0	10×10
Au	494	12.2	7.0	10×10
Cu	390	12.2	7.0	10×10

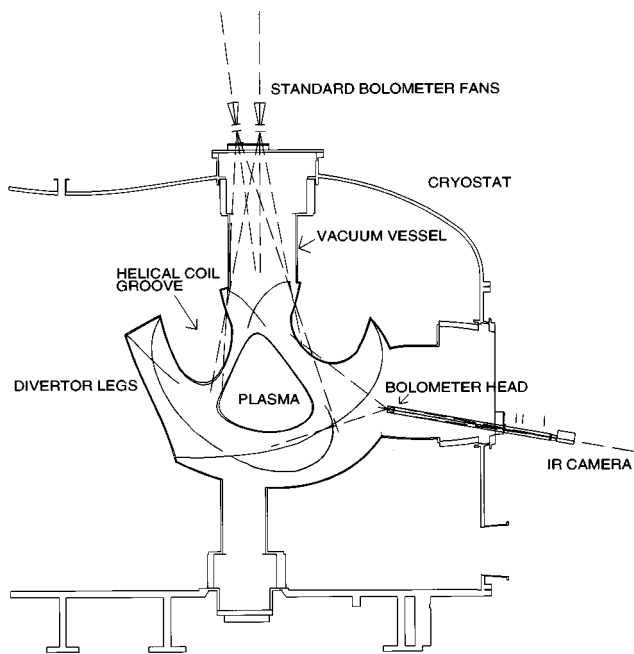


FIG. 1. Side view cross section of the LHD machine between port sections 4 and 3, showing possible locations of standard bolometer arrays (top) and imaging bolometer prototype (side). The slice is slightly tangential, hence the triangular-shape plasma cross section.

resulting mostly from the 1-cm-diam pinhole. The rise time is also dependent on the “distance” to the cooling block, and so could be increased at the expense of larger foils, even for a “fast” material such as copper.

Table II shows the foil diameter necessary to achieve a temperature rise time equal to the camera time resolution for a 2- $\mu\text{m}$ -thick foil of various materials, as well as the resulting maximum temperature. From this comparison we can also see that bismuth is the best candidate, in that it has a

large temperature rise for a reasonably sized foil segment. Titanium and Stainless 304 have similar sizes as the bismuth case but about half the temperature rise. The nickel foil segment has a diameter about twice the case of bismuth with about a third of the temperature rise, when the diameter is chosen to force the same rise time. Gold, aluminum, and copper have a slightly larger temperature rise to bismuth, but at the expense of only 20 cm spatial resolution in the plasma, due to room for fewer “foil segments.” The number of segments is constrained by the available transverse size for the diagnostic, which is coupled to port and flange dimensions or, ultimately, the number of resolution elements in the IR camera.

In order to obtain a sufficiently wide field of view (FOV) of the plasma, and also to obtain a high power loading on the foil (to be able to resolve the  $\Delta T$  with the IR cameras presently available), we need to insert the pinhole camera head in a reentrant configuration in the LHD vacuum vessel/dewar. This is sketched using a partly tangential sight line, as projected in a side view, shown in Fig. 1. The side port is used by the imaging bolometer, and we also show possible locations at the top of the machine for conventional bolometer arrays. The particular projection we have chosen (from port section 4 towards port section 3 on LHD) accounts for the triangular-shaped plasma cross section. A radial view would encounter a more elliptical shape. We are constrained to view the pinhole camera backside of the foil through a 102-mm-diam infrared window (either sapphire or zinc selenide), which will be mounted in a standard 152 mm Conflat vacuum flange with an intervening gate valve to be able to isolate or change out the window, without breaking vacuum.

A conceptual 3D view of the apparatus is shown in Fig. 2, where the essential elements of the diagnostic are de-

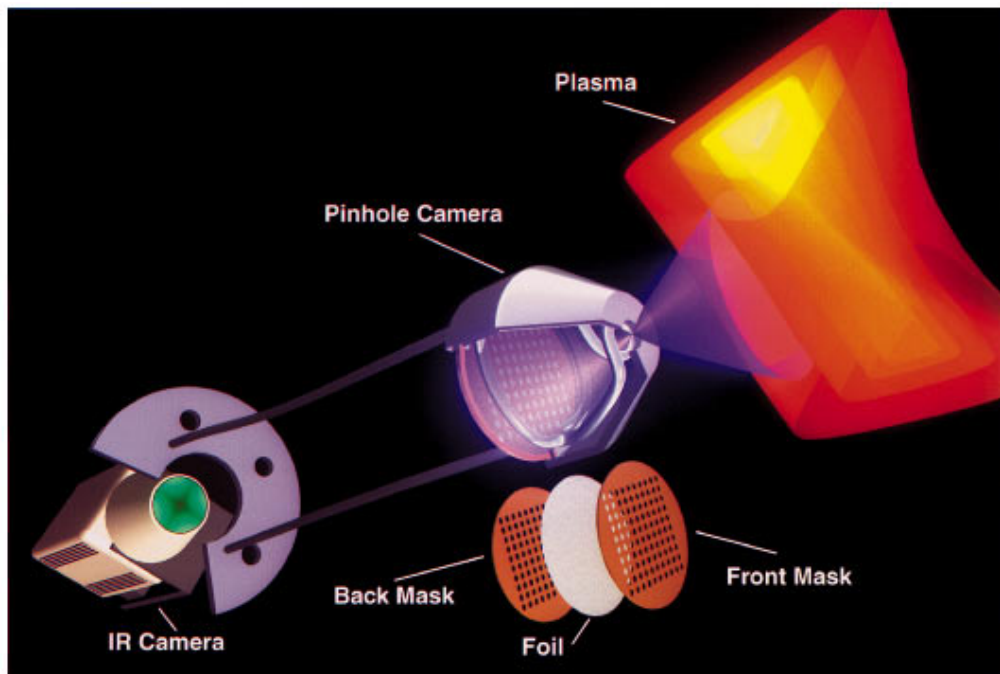


FIG. 2. Artist's view of the imaging bolometer prototype.

picted. The pinhole-camera head is water cooled by water flow in the stainless steel hollow tubing support struts, which also serve as mounting points for the pinhole camera assembly. No in-vessel welds or breaks in the cooling line are required, as we intend to use an integral cooling loop, to reduce any possibility of a water leak. The front and back foil masks will be oxygen-free high-conductivity copper (OFHC) sheets ( $\sim 2$  mm thick), with an appropriate ( $16 \times 16$ , for example) number of holes to form the segmented matrix. The relatively thick copper provides the thermal isolation between the adjacent "macropixels" or foil segments. To simplify construction, the sensor material will be one continuous sheet, with thickness chosen between 1 and 5  $\mu\text{m}$ . The IR camera (a  $256 \times 256$  element InAs array) has a FOV of  $2.23^\circ$  when used in conjunction with a commercially available 250 mm lens, which gives a 10-cm-wide view of the back copper mask from a focal distance of 2.6 m. The diameter of the pinhole-camera pinhole of 9.9 mm, at a minor radius of 2.0 m, gives a power flux of  $4.0 \text{ mW/cm}^2$  at the foil location, assuming a flat 100% radiation profile from a 3 MW plasma. This solution is nicely matched to a segmented foil size of 1.5 mm for bismuth, easily allowing a  $16 \times 16$  array to fit within the IR camera 10-cm-wide FOV, with a substantial length of copper between each foil segment for thermal isolation and cooling. The nonuniform temperature on the face of each foil segment will be mapped to 5 pixels on the IR camera. For the 15 ms time constant and pinhole described above, the detection limit<sup>5</sup> would be  $250 \mu\text{W/cm}^2$  using our existing Amber IR camera, or even  $2.5 \times$  smaller with a state-of-the-art  $\pm 0.01^\circ\text{C}$  resolution IR system. For monitoring the thermal drift of the copper masks, either foil segments that don't view the plasma, or a conventional thermocouple, or both, could be used.

#### IV. SUMMARY

We have outlined a design for an imaging bolometer system, capable of steady-state operation, to be installed on

the LHD stellarator. Because of recent advances in infrared imaging technology, it is now possible to use remote-sensing techniques to monitor small temperature rises in a segmented foil, and therefore actually build a simple, multichannel diagnostic to image the radiation emitted by complex geometry plasmas. In a situation with a severe neutron and gamma environment, and difficult access for conventional wiring harnesses, (i.e., ITER), it is straightforward to envision a metal mirror transport relay to bring the IR image out to a protected position where the sensitive (and expensive) solid-state IR camera could be located. A low-cost, simpler, multichannel bolometer is the chief benefit to this approach, compared to conventional methods. We intend to build and demonstrate this prototype first on the LHD stellarator, as a collaborative U.S./Japan effort.

#### ACKNOWLEDGMENTS

This work is supported by the U.S. DOE Contract No. W-7405-ENG-36, and under auspices of the U.S./Japan Fusion Collaboration Program No. FuY-96 P300.

- <sup>1</sup>O. Motojima *et al.*, *Fusion Eng. Des.* **20** (1993).
- <sup>2</sup>D. V. Orlinskij and G. Magyar, *Nucl. Fusion* **28**, 664 (1988).
- <sup>3</sup>J. Shivell, G. Renda, J. Lowrance, and H. Hsuan, *Rev. Sci. Instrum.* **53**, 1527 (1982).
- <sup>4</sup>G. Miller, J. C. Ingraham, and L. S. Schrank, *Rev. Sci. Instrum.* **53**, 1410 (1982).
- <sup>5</sup>K. F. Mast *et al.*, *Rev. Sci. Instrum.* **56**, 969 (1985).
- <sup>6</sup>A. W. Leonard, W. H. Meyer, B. Geer, D. M. Behne, and D. N. Hill, *Rev. Sci. Instrum.* **66**, 1201 (1995).
- <sup>7</sup>G. A. Wurden, in *Diagnostics for Experimental Thermonuclear Fusion Reactors*, edited by P. E. Scott *et al.* (Plenum, New York, 1996), pp. 603–606.
- <sup>8</sup>B. J. Peterson and S. Sudo, "Plans for Two-Dimensional Steady-State Bolometric Measurements on LHD," paper B26-P2-23, Toki, Japan. ITC-7 Conference, Nov. 30, 1995 (to be published).
- <sup>9</sup>M. N. Ozisik, *Boundary Value Problems of Heat Conduction* (International Textbook, Scranton, 1968), Eq. 3–100, p. 152.
- <sup>10</sup>F. Kreith and W. Z. Black, *Basic Heat Transfer* (Harper and Row, New York, 1980), Appendix E, pp. 508–513.